

Molecular simulation study on phase separation of immunoglobulin G

Lv-Meng Hu(胡吕梦), Yuan-Qiang Chen(陈远强), Hong-Ming Ding(丁泓铭), and Yu-Qiang Ma(马余强)
Citation: Chin. Phys. B, 2025, 34 (**8**): 088701. DOI: 10.1088/1674-1056/add50b
http://cpb.iphy.ac.cn; http://iopscience.iop.org/cpb

What follows is a list of articles you may be interested in

Depolymerization mechanism of microtubule revealed by nucleotide-dependent changes of longitudinal and lateral interactions

Bingbing Zhang(张冰冰), Ziling Huo(霍子玲), Jiaxi Li(李佳希), Jingyu Qin(覃静宇), and Yizhao Geng(耿轶钊)
Chin. Phys. B, 2025, 34 (**6**): 068702. DOI: 10.1088/1674-1056/adc369

Effects of palmitoylation on membrane protein partitioning into lipid domains in model cellular membranes

Shishi Wu(吴施施) and Qing Liang(梁清)
Chin. Phys. B, 2025, 34 (**5**): 058701. DOI: 10.1088/1674-1056/adbee9

Tail-structure regulated phase behaviors of a lipid bilayer

Wenwen Li(李文文), Zhao Lin(林召), Bing Yuan(元冰), and Kai Yang(杨恺)\ccclink
Chin. Phys. B, 2020, 29 (**12**): 128701. DOI: 10.1088/1674-1056/abad20

Combined effects of headgroup charge and tail unsaturation of lipids on lateral organization and diffusion of lipids in model biomembranes

Xiao-Jie Chen(陈晓洁), Qing Liang(梁清)
Chin. Phys. B, 2017, 26 (**4**): 048701. DOI: 10.1088/1674-1056/26/4/048701

Multiscale molecular dynamics simulations of membrane remodeling by Bin/Amphiphysin/Rvs family proteins

Chun Chan(陈骏), Haohua Wen(文豪华), Lanyuan Lu(鲁兰原), Jun Fan(范俊)
Chin. Phys. B, 2016, 25 (**1**): 018707. DOI: 10.1088/1674-1056/25/1/018707

RAPID COMMUNICATION

Molecular simulation study on phase separation of immunoglobulin G

Lv-Meng Hu(胡吕梦)[1], Yuan-Qiang Chen(陈远强)[1], Hong-Ming Ding(丁泓铭)[1,†], and Yu-Qiang Ma(马余强)[2,3]

[1] *Center for Soft Condensed Matter Physics and Interdisciplinary Research, School of Physical Science and Technology, Soochow University, Suzhou* 215006, *China*
[2] *National Laboratory of Solid State Microstructures and Department of Physics, Collaborative Innovation Center of Advanced Microstructures, Nanjing University, Nanjing* 210093, *China*
[3] *Jiangsu Physical Science Research Center, Nanjing* 210093, *China*

(Received 2 April 2025; revised manuscript received 28 April 2025; accepted manuscript online 7 May 2025)

Understanding the liquid–liquid phase separation (LLPS) of immunoglobulin G (IgG) is crucial, as it profoundly influences IgG's biological activity and stability. In this study, we employed coarse-grained molecular dynamics simulations to systematically investigate the phase separation behavior of IgG. We first constructed two types of IgG models: all-pair IgG model and partial-pair IgG model, and compared the coexistence curve from our simulations with experimental data. Our results showed that the partial-pair IgG model aligns better with the experimental critical temperature and critical density. Using this model, we then calculated the temperature-dependent variations of IgG's radius of gyration, surface tension, viscosity, etc. More importantly, we demonstrated that variations in the interaction strengths among IgG molecules significantly influence their phase separation behavior. Specifically, a higher standard deviation of interaction strength at different temperatures is found to lead to more stable phase-separated states. Furthermore, we observed that the introduction of repulsive polymers and strongly attractive polymers consistently enhances IgG phase separation, while weakly attractive polymers exhibit a dual regulatory effect on the phase separation. Overall, this study provides valuable insights into the mechanisms governing IgG phase behavior, with potential implications for optimizing biopharmaceutical products.

Keywords: phase separation, immunoglobulin G, coarse-graining, molecular dynamics

PACS: 87.10.Tf, 64.75.–g, 87.15.–v, 87.15.A–

DOI: 10.1088/1674-1056/add50b **CSTR:** 32038.14.CPB.add50b

1. Introduction

Immunoglobulin G (IgG) is the most important type of antibody in the human body, accounting for approximately 70%–80% of total antibodies.[1] It is primarily synthesized by plasma cells and plays a crucial role in immune function, including neutralizing pathogens, promoting phagocytosis, and activating the complement system.[1–3] In recent years, IgG has garnered significant attention, particularly in the context of its liquid–liquid phase separation (LLPS), a key biophysical phenomenon that profoundly affects its biological activity and stability,[4–10] which represents a key step in the study of therapeutic antibody formulations.[11,12] LLPS occurs when IgG spontaneously separates into dilute and concentrated phases under specific conditions, impacting protein solubility, functionality, and overall stability.[13–15] Therefore, investigating the mechanisms of IgG phase separation holds considerable significance for both fundamental biophysical research and the development of biopharmaceutical products.[16,17]

In recent years, significant progress has been made in experimental studies on the phase separation of IgG, which is influenced by multiple factors,[18–23] with intermolecular interactions playing a dominant role in determining the phase diagram structure.[24–26] These interactions include contributions from excluded volume effects, electrostatic interactions, and short-range interactions.[27–29] Additionally, external conditions such as temperature, pH, ionic strength, and the type and concentration of additives also play a critical role in this process.[30–32] For example, Wang *et al.*[24] found that IgG exhibits a broad and asymmetric coexistence curve compared to globular proteins, with a critical concentration of approximately 100.00 mg/ml. In another noteworthy study, Mason *et al.*[6] emphasized that the pH and ionic strength of the solution are two key factors influencing the stability of protein solutions. Furthermore, Nishi *et al.*[19] indicated that at high ionic concentrations, the stability of IgG solutions is less sensitive to pH, whereas at low ionic strength, phase separation is more stable under acidic conditions.

However, due to the complexity of experimental conditions, understanding these phenomena solely through experiments poses challenges. To address this, the present study employs coarse-grained molecular dynamics (CGMD)[33] simulations to explore the microscopic mechanisms underlying protein multibody interactions behind existing experimen-

[†]Corresponding author. E-mail: dinghm@suda.edu.cn

© 2025 Chinese Physical Society and IOP Publishing Ltd. All rights, including for text and data mining, AI training, and similar technologies, are reserved.

tal observations. We constructed a 12-bead model of IgG molecules and compared our model's coexistence curve with experimental data to determine the interaction parameters between the coarse-grained IgG beads. We further analyzed various properties of IgG molecules, including the radius of gyration, radial distribution function, surface tension, diffusion coefficient, and viscosity. Finally, we also examined the energy dispersity of the IgG system and investigated the influence of external molecules on IgG phase separation behavior.

2. Model and methods

2.1. Coarse-grained model for IgG

The structure of IgG consists of four polypeptide chains: two heavy chains and two light chains, connected by disulfide bonds, forming a classic Y-shaped structure. As shown in Fig. 1(a), each heavy chain contains four domains: one variable domain (V_H) and three constant domains (C_{H1}, C_{H2}, and C_{H3}),[34–36] while each light chain contains two domains: a variable domain (V_L) and a constant domain (C_L). The C_{H2} and C_{H3} domains of the heavy chain form the Fc region, which is characterized by its crystallizable properties, while the Fab region, responsible for antigen binding, is composed of the V_H, V_L, and C_{H1} domains.[37,38] The V_H and V_L domains together form the antigen-binding site, which is crucial for specific antigen recognition. Additionally, the complementarity-determining regions (CDRs) within the variable domains are made up of amino acids encoded by highly variable segments from the human genome, resulting in a high diversity of antibodies.[39,40] The C_{H3} domains play a critical role in maintaining the stability of antibodies. Previous studies have shown that the structural stability of the C_{H3} domains significantly impacts the antigen-binding capability of the variable domains.[41,42] Conformational changes in the C_{H3} domains can affect interactions between V_L and V_H, ultimately impacting the antibody's overall functionality.[43]

As shown in Fig. 1(b), in the coarse-grained molecular dynamics (CGMD) simulations, we constructed a 12-bead coarse-grained (CG) IgG model to identify CG sites based on the centroids of IgG domains,[36] with different colors representing the molecular domains: V_H (blue), C_{H1} (red), C_{H2} (yellow), C_{H3} (green), V_L (cyan), and C_L (purple). Here, the C_{H1}, C_L, and C_{H2} domains of the IgG molecule are outlined with black dashed lines, dividing the IgG molecule into internal and external regions to facilitate the subsequent model setup. This model incorporates three standard types of effective interaction potentials: bond, angle, and dihedral. The bond potential applies to two CG beads, while angle and dihedral potentials act on three and four CG beads, respectively. For bond interactions, we introduced the Urey–Bradley (UB) potential. The interactions for bonds, angles, and dihedrals are defined using harmonic approximations of interaction strengths[36]

$$V(r)_{\text{bond}} = k_{\text{bond}}\,(r - r_0)^2\,, \tag{1}$$

$$V(\theta)_{\text{angle}} = k_{\text{angle}}(\theta - \theta_0)^2 + k_{\text{UB}}(r - r_{\text{UB}})^2, \tag{2}$$

$$V(\Phi)_{\text{dihedral}} = k_{\text{dihedral}}\left[1 + \cos\left(\Phi_0 - d\right)\right], \tag{3}$$

where r is the distance between two beads in a bond, θ is the angle between three beads, and Φ is the dihedral angle in a set of four beads. And k_{bond}, k_{angle}, k_{UB}, and k_{dihedral} are the spring constants for bond, angle, Urey–Bradley (UB), and dihedral interactions, respectively. r_0, r_{UB}, and the angles θ_0 and Φ_0 are parameters of the CG model. The UB term adds an additional interaction between the first and third beads in an angle. The detailed parameters for the IgG model can be found in the previous work by Chaudhri *et al.*,[36] where they were obtained via direct Boltzmann inversion using all-atom simulations of a single IgG molecule. In their approach, dimensionless units were employed to calculate the model's overall volume based on the partial specific volume v, under the assumption that all coarse-grained (CG) sites occupy identical volumes. Using this methodology, we determined the diameter σ of the coarse-grained bead for IgG, as defined by

$$\sigma = 2\left(\frac{mv}{N}\frac{3}{4\pi}\right)^{\frac{1}{3}}, \tag{4}$$

where m is the protein molecular weight, N is the number of CG beads (12 for the IgG molecular model), and $v = 0.729$ mL/g.[44] The calculated diameter of the IgG beads is $\sigma_{\text{IgG}} = 30.38$ Å.

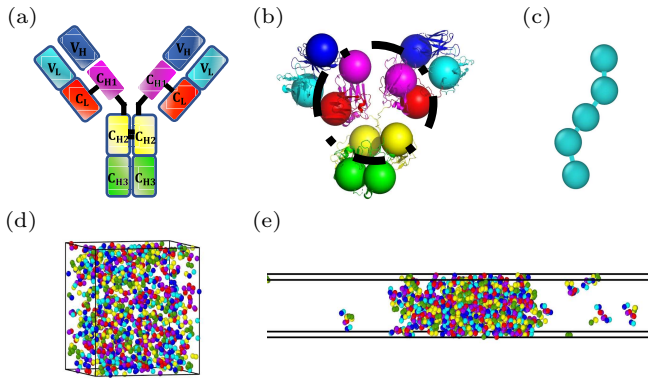


Fig. 1. Schematic representation of the coarse-grained models of IgG and polymer used in the simulations. (a) Structural schematic of IgG, which consists of two identical heavy chains (V_H–C_{H1}–C_{H2}–C_{H3}) and two identical light chains (V_L–C_L). (b) The 12-bead coarse-grained model overlaid on the 3D structure of IgG, where the C_{H1}, C_L, and C_{H2} domains of the IgG molecule are outlined by black dashed lines. The diameter of the coarse-grained beads is $\sigma_{\text{IgG}} = 30.38$ Å. (c) Coarse-grained model of polymer, where the coarse-grained bead diameter is $\sigma_{\text{polymer}} = 13.75$ Å. (d) Snapshot of the simulation box with IgG in a homogeneous phase at the initial state. (e) A snapshot of the dense phase of IgG molecules in a slab simulation box.

In the IgG model, the non-bonded beads interact through the Lennard–Jones (LJ) potential, which is defined as

$$U_{\text{LJ}} = 4\varepsilon\left[\left(\frac{\sigma}{r}\right)^{12} - \left(\frac{\sigma}{r}\right)^{6}\right] + \varepsilon, \tag{5}$$

where ε is the energy well depth and σ represents the bead diameter. In this study, we considered two coarse-grained models of IgG. The first model configures all molecular sites to interact with mutual attraction through the LJ potential. This model is defined as the 'all-pair IgG model'. The second model builds upon the above model by introducing repulsive interactions between specific internal structural domains of the IgG molecule, including the C_{H1}, C_{H2}, and C_L regions. Specifically, the interactions between these coarse-grained beads (C_{H1}, C_{H2}, and C_L) were modeled using the Weeks–Chandler–Andersen (WCA) potential, a purely repulsive potential defined as

$$V_{\mathrm{WCA}}(r) = \begin{cases} 4\varepsilon\left[\left(\frac{\sigma}{r}\right)^{12} - \left(\frac{\sigma}{r}\right)^{6}\right] + \varepsilon, & \text{if } r < r_{\mathrm{c}}, \\ 0, & \text{if } r \geq r_{\mathrm{c}}, \end{cases} \tag{6}$$

where r denotes the inter-bead distance, and all beads within the coarse-grained (CG) model are assumed to have uniform dimensions. The strength of the repulsive interactions is quantified by setting $\varepsilon = 1\ k_{\mathrm{B}}T$, with a cutoff radius $r_{\mathrm{c}} = 2^{1/6}\sigma_{\mathrm{IgG}}$. This model is referred to as the 'partial-pair IgG model'.

2.2. Coarse-grained model for polymer

Polymers have been extensively utilized in biochemical and pharmaceutical applications due to their excellent biocompatibility with cellular components.[45,46] Recent studies have demonstrated their widespread adoption as model additives for investigating liquid–liquid phase separation of biomacromolecules.[47–49] Therefore, we developed a coarse-grained polymer model to investigate its regulatory effects on IgG phase separation.

In our simulations, we took the polyethylene glycol (PEG) with a molecular weight of 5000 Da as an example, and constructed a coarse-grained polymer model composed of five equivalent beads (Fig. 1(c)), where each bead represents multiple repeating units (corresponding to a molecular weight of 1000 Da). Using

$$R_{\mathrm{F}} = \alpha N^{3/5}, \tag{7}$$

we calculated the distance between each bead to be 22.36 Å, where N represents the degree of polymerization, and α refers to the monomer size (approximately 3.5 Å for PEG). The diameter of the coarse-grained beads was determined to be $\sigma_{\mathrm{polymer}} = 13.75$ Å, using the formula in Eq. (4). Here, m denotes the molecular weight of the polymer, N indicates the number of CG beads (which is 5 for the polymer) and $v = 0.820$ mL/g.[50] The bond potential between the coarse-grained beads is defined using a harmonic approximation

$$V(r)_{\mathrm{bond}} = k_{\mathrm{bond}}(r - r_0)^2, \tag{8}$$

with a spring constant $k_{\mathrm{bond}} = 1500\ k_{\mathrm{B}}T/\sigma^2$ and an equilibrium distance $r_0 = \sigma_{\mathrm{polymer}}$.

2.3. Slab method

To accurately characterize the phase diagram of IgG, we employed the slab method to simulate the phase separation phenomena of IgG at various temperatures.[51,52] Simulations were performed using the LAMMPS software package (29 October 2020),[53] with Langevin dynamics employed in the NVT ensemble. The initial dimensions of the simulation box were set to $30\sigma \times 30\sigma \times 30\sigma$, containing a total of 100 IgG molecules randomly distributed throughout the simulation box [Fig. 1(d)]. To simplify calculations, we adopted a dimensionless Lennard–Jones unit system, where energy is expressed in terms of $k_{\mathrm{B}}T$, temperature as $T^* = k_{\mathrm{B}}T/\varepsilon$, distance as σ_{IgG}. The time step used in the simulations was set to 0.00002τ. All simulations were conducted under periodic boundary conditions. To obtain the density distribution of IgG chains along the z-axis, we scaled the dimensions of the initial cubic box to approximately 10σ in the x and y directions. An anisotropic pressure coupling was employed to equilibrate the system along the z-axis, expanding the box's z dimension to 100σ. The resulting slab simulation box, as illustrated in Fig. 1(e), displays a snapshot of the dense phase obtained at the initial temperature. Subsequently, the system was gradually heated to the target temperature, and after an equilibration duration of 4×10^8 time steps, the IgG density distribution was analyzed.

We initially centered the trajectory of each frame within the slab and divided the simulation box into 100 squares, each with a width of 1σ. The trajectories obtained from the slab method simulation (sampling one frame every 1000τ) were then centered within the slab, and subsequent averaging was performed on the trajectories. In the event of phase separation, the average density profile was fitted to a hyperbolic tangent function

$$\rho(z) = \frac{\rho_{\mathrm{D}} + \rho_{\mathrm{L}}}{2} - \frac{\Delta\rho}{2}\tanh\left(\frac{z - z_0}{d}\right), \tag{9}$$

where z_0 represents the position of the interface and d determines the interfacial thickness. The average concentrations of IgG in the dilute phase (ρ_{L}) and the dense phase (ρ_{D}) were computed accordingly. The critical temperature T_{c} and the critical concentration ρ_{c} were determined through fitting using

$$\rho_{\mathrm{D}} - \rho_{\mathrm{L}} = A\,(T_{\mathrm{c}} - T)^{\beta}, \tag{10}$$

$$\frac{\rho_{\mathrm{D}} + \rho_{\mathrm{L}}}{2} = \rho_{\mathrm{c}} + B\,(T_{\mathrm{c}} - T), \tag{11}$$

where β is the critical exponent, set at 0.325, which exhibits the universality of the three-dimensional Ising model.[51] A and B are the fitting parameters used to determine the critical points of the phase diagram.

2.4. Calculation of IgG structure and material properties

To further investigate the structural properties of IgG molecules, we analyzed the radius of gyration (R_g) of the IgG molecules, which is calculated using the following formula:

$$R_g = \sqrt{\frac{1}{N}\left\langle \sum_{i=1}^{N} (\boldsymbol{r}_i - \boldsymbol{r}_{COM})^2 \right\rangle}, \tag{12}$$

where N is the number of atoms in the structure, $\boldsymbol{r}_i$ is the position of atom i in 3D coordinates, and $\boldsymbol{r}_{COM}$ is the geometric center of the molecule. Notably, changes in the radius of gyration can reflect alterations in molecular conformation as a function of varying conditions such as temperature and concentration.

The radial distribution function (RDF) is calculated as

$$g(r) = \frac{\rho(r)}{\rho}, \tag{13}$$

where $\rho(r)$ refers to the local density at a distance r from a reference atom, and ρ represents the average density of the system.

During the phase separation of IgG, the surface tension γ at the interface between the concentrated and dilute phases is a significant determinant of fluidity.[54,55] We employed the Kirkwood–Buff[56] relation to calculate the surface tension

$$\gamma = \frac{L_z}{2}\left\langle P_{zz} - \frac{P_{xx}+P_{yy}}{2} \right\rangle, \tag{14}$$

where L_z denotes the length of the simulation box in the z-direction, and P_{xx}, P_{yy}, and P_{zz} refer to the pressure tensor components in the x, y, and z directions, respectively. The factor of 1/2 accounts for the presence of two interfaces in the slab geometry used for phase coexistence simulations.

The diffusion coefficient characterizes the mobility of molecules within the solution. In this study, we calculated it by monitoring the mean squared displacement (MSD) of IgG molecules as a function of time[57]

$$\mathrm{MSD}(t) = \left\langle [r_i(t) - r_i(0)]^2 \right\rangle = 6Dt, \tag{15}$$

where $r_i(t)$ represents the position of a polymer chain i at time t. In this work, the diffusion coefficients were calculated using PyLAT,[58] an analysis tool for LAMMPS.

For viscosity calculations, we employed the Green–Kubo (GK) formalism[59,60] to evaluate the viscoelastic behavior of IgG aggregates. In isotropic systems, the shear relaxation modulus $G(t)$ can be determined using all components of the stress tensor $\sigma_{\alpha\beta}$[59]

$$G(t) = \frac{V}{5\,k_B T}\left\{ \left\langle \sigma_{xy}(0)\,\sigma_{xy}(t) \right\rangle + \left\langle \sigma_{xz}(0)\,\sigma_{xz}(t) \right\rangle + \left\langle \sigma_{yz}(0)\,\sigma_{yz}(t) \right\rangle + \frac{1}{6}\left[\left\langle N_{xy}(0)\,N_{xy}(t) \right\rangle + \left\langle N_{xz}(0)\,N_{xz}(t) \right\rangle + \left\langle N_{yz}(0)\,N_{yz}(t) \right\rangle \right] \right\}, \tag{16}$$

where $N_{\alpha\beta} = \sigma_{\alpha\alpha} - \sigma_{\beta\beta}$ represents the normal stress difference. The relaxation modulus $G(t)$ was computed using the "Compute ave/correlation/long" command available in the "USER-MISC" package of LAMMPS software.[60] Subsequently, the shear viscosity η was determined by time integration of the shear stress relaxation modulus

$$\eta = \int_0^\infty G(t)\,\mathrm{d}t. \tag{17}$$

To address the typical noise characteristics observed in the terminal decay region of aggregates during simulations, $G(t)$ was fitted to a Maxwell model over longer timescales using the open-source RepTate software[61]

$$G(t) = \sum_{i=1}^{M} G_i \exp\left(-\frac{t}{\tau_i}\right), \tag{18}$$

where τ_i and G_i are the fitting parameters defined in the Maxwell modes, and M is the number of Maxwell modes used in the fitting. Overall, the viscosity was calculated by numerically integrating the initial region (0–t) using the trapezoidal rule and summing the contribution from the terminal region (t_0–∞), which corresponds to slower relaxation modes[11,62]

$$\eta = \eta(t_0) + \sum_{i=1}^{m} \tau_i G_i \exp\left(-\frac{t_0}{\tau_i}\right), \tag{19}$$

where $\eta(t_0)$ corresponds to the contribution computed over shorter timescales and t represents the transition time between the two regimes.

3. Results and discussion

3.1. Phase diagrams of IgG solutions in the all-pair IgG model

To investigate the phase separation behavior of IgG, we first performed simulations using the all-pair IgG model. In this model, all the beads in IgG molecules interact with each other through the Lennard–Jones potential with the interaction strength ε. We then generated phase diagrams under different conditions by tuning the interaction strength ε between beads. Previous experimental studies have shown that IgG phase separation exhibits unique characteristics, namely, the coexistence curve displays an asymmetric shape, with a critical temperature of approximately 273.00 K and a critical concentration of about 100.00 mg/ml.[24]

In our simulations, we varied the interaction strength ε between 0.20 $k_B T$ and 0.32 $k_B T$. As shown in Fig. 2(a), the density distribution of IgG along the z-axis obtained under an interaction strength of 0.30 $k_B T$ is presented. The distribution curves overlap at different temperatures and exhibit distinct peaks, indicating significant phase separation at these temperatures. As the temperature increases, the peak height decreases, reflecting a weakening of phase separation.

We then fitted the critical temperature T_c using Eq. (1), as shown in Fig. 2(b). The fitting yielded a critical temperature of $T_c = 272.60$ K. Using Eq. (11), we obtained the critical concentration ρ_c by fitting the data within the same temperature range, as shown in Fig. 2(c). This results in a critical density of $\rho_c = 192.50$ mg/ml. Figure 2(d) shows the phase diagram of IgG, with the relationship between the dense-phase and dilute-phase concentrations at each temperature, and the critical point obtained from the fitting. The inset rectangular box displays a snapshot of the phase separation observed at 217.50 K. The phase diagram clearly indicates that the calculated critical temperature here is consistent with experimental critical temperature (273.00 K), and the calculated coexistence curve also exhibits an asymmetric shape.[24]

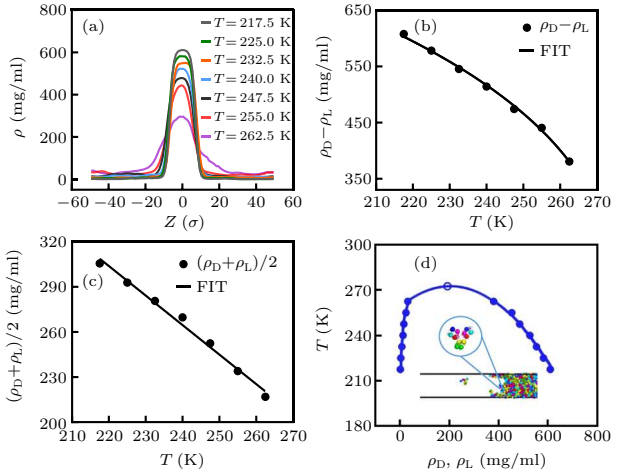


Fig. 2. Phase diagram at interaction strength $\varepsilon = 0.30\ k_BT$ of the all-pair IgG model. (a) Slab density distribution profiles at a series of coexistence temperatures for the all-pair IgG coarse-grained model, with an interaction strength of $\varepsilon = 0.30\ k_BT$ between all sites. (b) The critical temperature obtained from the fitted curve is 272.60 K. (c) The critical density obtained from the fitted curve is 192.50 mg/ml. (d) The coexistence curve of IgG LLPS obtained from the density distribution, with an inset showing a simulation snapshot of the IgG system at a temperature of 247.50 K.

The phase diagrams formed under different ranges of interaction strength (ε) are shown in Fig. 3(a). As the interaction strength increases, the coexistence curves shift toward the upper-right, indicating that stronger interactions significantly elevate the critical temperature (T_c) for IgG phase separation. Figure 3(b) illustrates the relationship between the critical temperature (T_c) and critical density (ρ_c) as a function of interaction strength. As the interaction strength increases, the critical temperature shows a linear upward trend, while the critical density exhibits a slight decrease. This observation aligns with the findings of Vlachy *et al.*,[63] who demonstrated that the critical volume fraction decreases with increasing ε based on Wertheim's thermodynamic perturbation theory. However, the critical density observed here is much higher than the experimental value of 100 mg/ml. Moreover, since ρ_c is relatively insensitive to variations in ε, it suggests that simply adjusting ε is unlikely to achieve experimental agreement for the critical density in simulations.

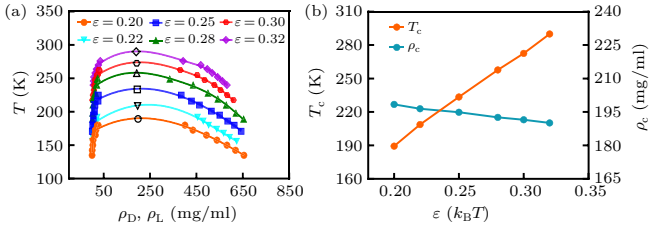


Fig. 3. Phase diagrams of the all-pair IgG model under different interaction strengths. (a) Comparison of phase diagrams obtained for the all-pair IgG model within the interaction strength range of $\varepsilon = 0.20\ k_BT$ to $0.30\ k_BT$. (b) Variation of the critical temperature (T_c) and critical concentration (ρ_c) of the all-pair IgG model as a function of interaction strength.

3.2. Phase diagrams of IgG solutions in the partial-pair IgG model

The all-pair IgG model assumed attractive interactions between all beads, which may be overly simplistic. Previous experimental studies have revealed that the interactions between C_{H1}, C_{H2}, and C_L domains exhibit weaker binding affinities, while the interactions between the C_{H3} domain and the variable domain (V_H and V_L) dominate the inter-protein interactions.[64,65] To capture this characteristic, we developed a 'partial-pair IgG model', allowing attractive interactions only between the coarse-grained sites in the V_H (blue), C_{H3} (green), and V_L (cyan) domains, as illustrated in Fig. 1(b). The interactions between these beads and other beads, and the interactions among other beads were repulsive via WCA potential.

Following the same approach as before, we simulated the phase separation behavior of IgG using the partial-pair IgG model, tuning the interaction strength ε in the range of $0.70\ k_BT$ to $0.90\ k_BT$. The results for $\varepsilon = 0.82\ k_BT$ are shown in Fig. 4(a), which displays the density distribution of IgG molecules along the z-axis at different temperatures. As the temperature increases, the peak height decreases, indicating a gradual reduction in the extent of phase separation. Using an appropriate temperature range and fitting data with Eq. (10), the critical temperature was determined to be 272.60 K, as shown in Fig. 4(b). The linear decrease in the average density of the dense and dilute phases with increasing temperature is illustrated in Fig. 4(c). Fitting this trend using Eq. (11), we obtained the critical concentration as 125.63 mg/ml. The relationship between the dense-phase and dilute-phase concentrations at each temperature was plotted as a phase diagram, with the critical point obtained earlier [Fig. 4(d)]. The phase separation process across varying temperatures is clearly demonstrated, and from top to bottom, as the temperature increases, in Fig. 4(e). The IgG molecular system transitions toward a uniform distribution, reflecting the system's approach to the critical point of the phase diagram.

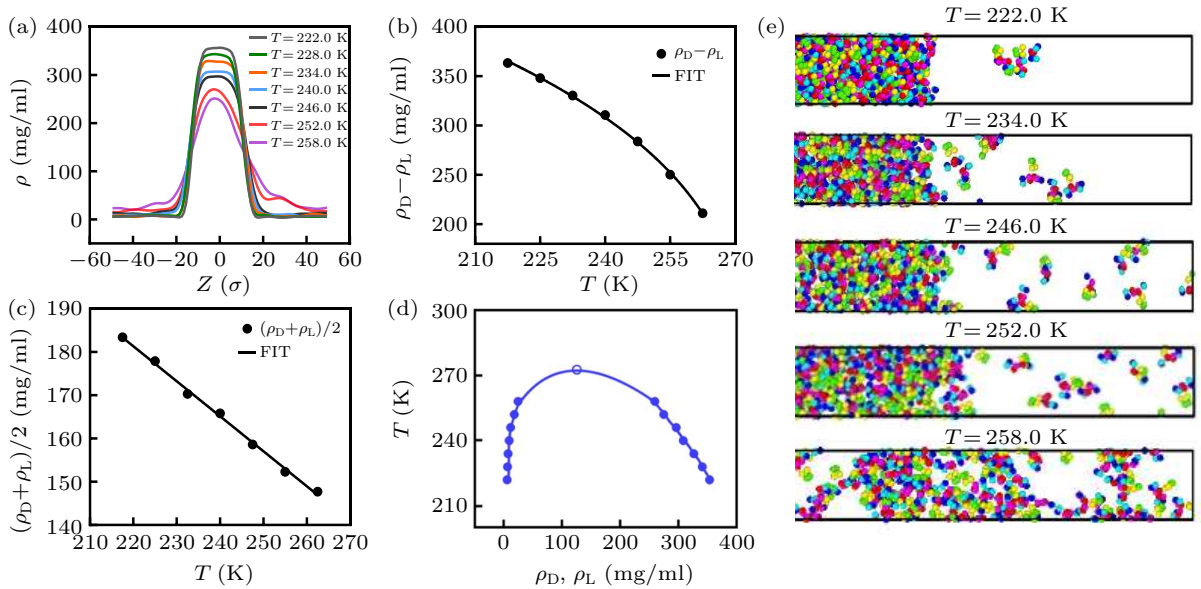


Fig. 4. Phase diagram at interaction strength $\varepsilon = 0.82\ k_BT$ of the partial-pair IgG model. (a) Density distribution profiles at various temperatures obtained for the partial-pair IgG model with an interaction strength of 0.82 k_BT. (b) The fitted critical temperature curve, yielding a critical temperature of 272.60 K. (c) The fitted critical density curve, yielding a critical density of 125.63 mg/ml. (d) The LLPS coexistence curve of IgG derived from density distributions at different temperatures. (e) Simulation snapshots of the partial-pair IgG IgG model at an interaction strength of $\varepsilon = 0.82\ k_BT$, showing a gradual approach to the critical point from top to bottom.

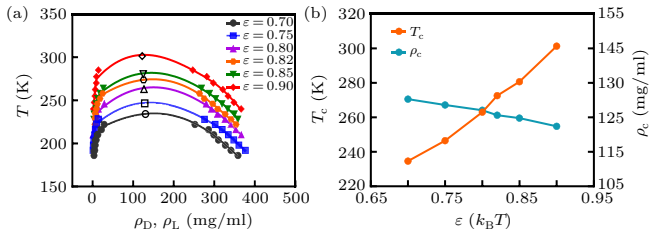


Fig. 5. Phase diagrams of the partial-pair IgG model under different interaction strengths. (a) Comparison of phase diagrams obtained for the partial-pair IgG model within the interaction strength range of $\varepsilon = 0.70\ k_BT$ to $0.90\ k_BT$. (b) Variation of the critical temperature (T_c) and critical concentration (ρ_c) of the partial-pair IgG model as a function of interaction strength.

The comparative phase diagrams obtained for the partial-pair IgG model under interaction strengths ranging from 0.70 k_BT to 0.90 k_BT are shown in Fig. 5(a). Consistent with the results from the all-pair IgG model, the coexistence curves shift upward with increasing interaction strength, indicating enhanced phase separation ability. Figure 5(b) illustrates the trends in critical temperature and critical concentration as a function of interaction strength. The critical temperature increases significantly with stronger interactions, suggesting that enhanced attractive forces can sustain phase separation at higher temperatures. Meanwhile, the critical concentration shows a slightly decreasing trend as the interaction strength increases. The results indicate that the critical temperature (272.60 K) and critical concentration (125.63 mg/ml) obtained at $\varepsilon = 0.82\ k_BT$ are the closest to the experimental data, suggesting that this model better captures the key features of IgG intermolecular interactions under realistic conditions. However, it is worth noting that the critical concentration still slightly deviates from the experimental value of 100.00 mg/ml. This discrepancy may stem from the model's assumption of equal interaction strength among the six attractive sites, as previous theoretical studies have indicated that the asymmetry in interaction strength between Fab and Fc regions could further reduce the critical concentration.[63,66] Here, for the sake of simplicity, we did not further modify the interaction strengths between the Fab and Fc regions, as their exact interaction strengths, or even their relative strengths, are difficult to determine experimentally and challenging to map onto our coarse-grained simulation model.

3.3. Structural and material properties of IgG molecules

To further investigate the phase behavior of IgG molecules, we selected the partial-pair IgG model with the interaction strength $\varepsilon = 0.82\ k_BT$, which aligns well with experimental results, to study the effect of temperature variations on the structural and thermodynamic properties of IgG molecules. We first calculated the radius of gyration R_g, which is used to measure the overall size and conformation of IgG molecules. Figure 6(a) shows the relationship between the average radius of gyration of a single IgG molecule and that of the IgG molecules in the phase-separated state as a function of temperature. It is found that the radius of gyration of a single molecule remains largely stable, indicating that temperature changes have minimal impact on the conformation of a single IgG molecule. In contrast, the average radius of gyration for the IgG system in the phase-separated state increases with temperature. This value is smaller than that of a single molecule, suggesting that the close packing of IgG molecules during phase separation leads to a more compact structure. We then calculated the radial distribution function (RDF) that

describes the spatial arrangement and interaction strength between molecules. Figure 6(b) illustrates how the RDF for IgG molecules in the phase-separated state varies with temperature. As the temperature increases, the peak of the RDF decreases, indicating a weakening of the ordered structure between IgG molecules at higher temperatures.

We next calculated the surface tension (γ) of IgG solutions using the slab method and Eq. (14). As shown in Fig. 6(c), the surface tension decreases with increasing temperature, suggesting a tendency toward interfacial instability as phase separation is reduced. Notably, the simulated surface tension values exhibit good agreement with experimental data,[67] both in terms of magnitude and temperature-dependent trends. This confirms the accuracy of our computational model in describing IgG's interfacial dynamics under thermal variations.

Interestingly, as shown in Fig. 6(d), we observed a power-law relationship for surface tension against the reduced temperature ($t = 1 - T/T_c$) near the critical temperature

$$\gamma = \gamma_0 t^{\mu}, \tag{20}$$

where γ_0 represents the critical surface tension, and we have assumed $\mu = 1.26$ based on Widom's hyperscaling relationship for the three-dimensional Ising model universality class.[68] The fitting parameters in Eq. (20) were $T_c = 272.10$ K. Notably, the critical temperature obtained by fitting the surface tension is close to that (272.60 K) by fitting the densities.

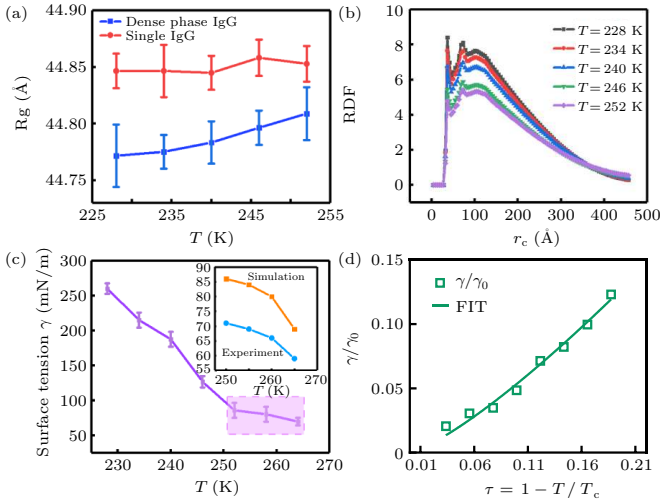


Fig. 6. Analysis of the structural properties and surface tension of the IgG model with an interaction strength of $\varepsilon = 0.82\, k_B T$. (a) The variation of the radius of gyration (R_g) of a single IgG molecule and the average radius of gyration (R_g) of IgG in the dense phase as functions of temperature. (b) The variation of the radial distribution function (RDF) of IgG in the dense phase during phase separation as a function of temperature. (c) Surface tension at different temperatures. The inset graph shows the simulated and experimental values[67] of the surface tension of the IgG. (d) Surface tension values (γ_0) scaled by the critical amplitude, fitted to the universal curve, showing the temperature dependence of surface tension as the temperature decreases, with simulation data points compared to theoretical predictions (blue curve).

To gain deeper insights into the material properties of the IgG molecules in dense phase, we further calculated the diffusion coefficients and viscosity. Figure 7(a) shows the mean squared displacement (MSD) of the center of mass of the IgG model as a function of time at different temperatures. The MSD vs. time curve is linear at the latter part of time scales. Based on this, the diffusion coefficients at different temperatures were calculated using Eq. (15), as shown in Fig. 7(b). This method of calculating the diffusion coefficient (D) from the MSD accurately captures the translational motion of IgG molecules within the dense phase and demonstrates that the diffusion coefficient increases consistently with rising temperature. Viscosity is a fundamental material property of biomolecular condensates. To further evaluate the viscosity of the IgG system, we employed the Green–Kubo (GK) relation. Figure 7(c) illustrates the shear stress relaxation modulus $G(t)$ as a function of time at different temperatures. Notably, $G(t)$ exhibits a sharp decay in the terminal region, indicating liquid-like behavior and complete relaxation of the IgG system. Subsequently, we performed a time integration based on Eq. (19) to calculate the viscosity (η) at different temperatures. As shown in Fig. 7(d), the viscosity decreases progressively with increasing temperature.

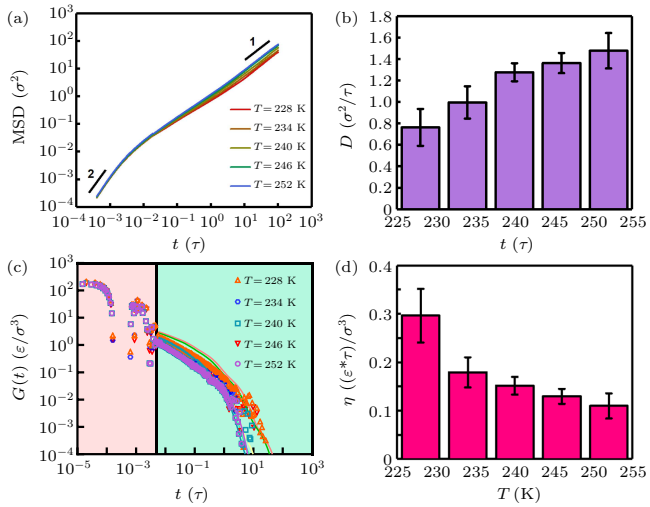


Fig. 7. Analysis of the material properties of the IgG model with an interaction strength of $\varepsilon = 0.82\, k_B T$. The variation of the (a) mean squared displacement (MSD), (b) diffusion coefficient (D), (c) shear stress relaxation modulus $G(t)$, and (d) shear viscosity (η) of the dense phase of IgG phase separation as functions of temperature.

3.4. Effect of dispersity of interaction strengths on IgG phase separation

In the above sections, we assumed that the system contained only one type of IgG molecule, meaning that the interactions between IgG beads were uniform. However, it is known that IgG molecules consist of variable domains (V_H and V_L), where the amino acid sequences are highly variable. This variability may lead to diversity in IgG interactions, even among IgG molecules of the same class.[69,70] To explore how

the dispersity of interaction strengths between IgG molecules affects their phase separation, we assumed that the interaction strengths (ε) within the IgG molecules follow a normal distribution with a mean of 0.82 $k_{\mathrm{B}}T$ and standard deviations of $\delta = 0.05\ k_{\mathrm{B}}T$, $0.10\ k_{\mathrm{B}}T$, $0.20\ k_{\mathrm{B}}T$, $0.30\ k_{\mathrm{B}}T$, and $0.40\ k_{\mathrm{B}}T$.

The maximum cluster interaction intensity distribution at temperature $T = 210$ K is shown in Fig. 8. When $\delta = 0.00\ k_{\mathrm{B}}T$ (i.e., the case in Subsections 3.2 and 3.3), the system forms a large, concentrated, and relatively uniform cluster, with a maximum cluster ratio of 0.77. At $\delta = 0.05\ k_{\mathrm{B}}T$ and $0.10\ k_{\mathrm{B}}T$, the cluster structure starts to disperse, though it remains relatively large, with a slight decrease in the maximum cluster ratio.

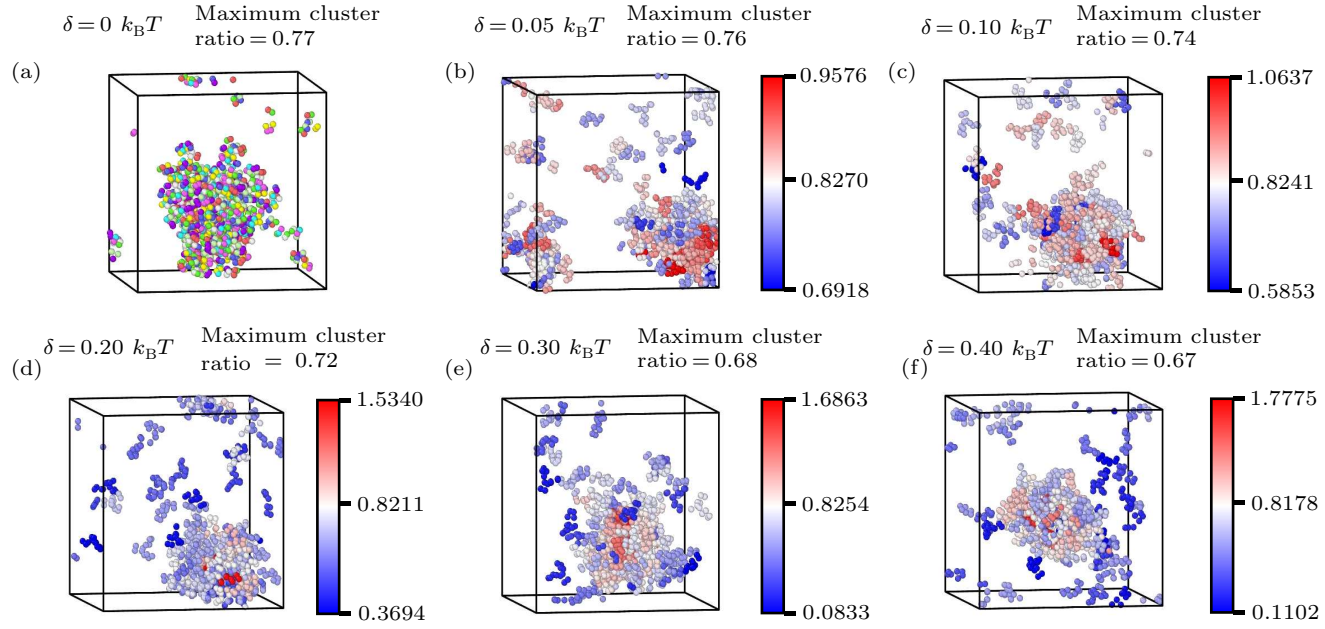


Fig. 8. The variation of the maximum cluster ratio and phase separation snapshots with the standard deviation at a temperature of $T = 210$ K. The intermolecular interaction strength in the IgG system has a mean value of 0.82 and standard deviations of (a) $0.00\ k_{\mathrm{B}}T$, (b) $0.05\ k_{\mathrm{B}}T$, (c) $0.10\ k_{\mathrm{B}}T$, (d) $0.20\ k_{\mathrm{B}}T$, (e) $0.30\ k_{\mathrm{B}}T$, and (f) $0.40\ k_{\mathrm{B}}T$. The color scale range varies from blue (weak interactions) to red (strong interactions). Clusters are defined using a distance-based criterion: two IgG molecules are considered part of the same cluster if any pair of interacting beads between them are within a cutoff distance of $2^{1/6}\sigma_{\mathrm{IgG}}$. The maximum cluster ratio is defined as the proportion of IgG molecules belonging to the largest cluster.

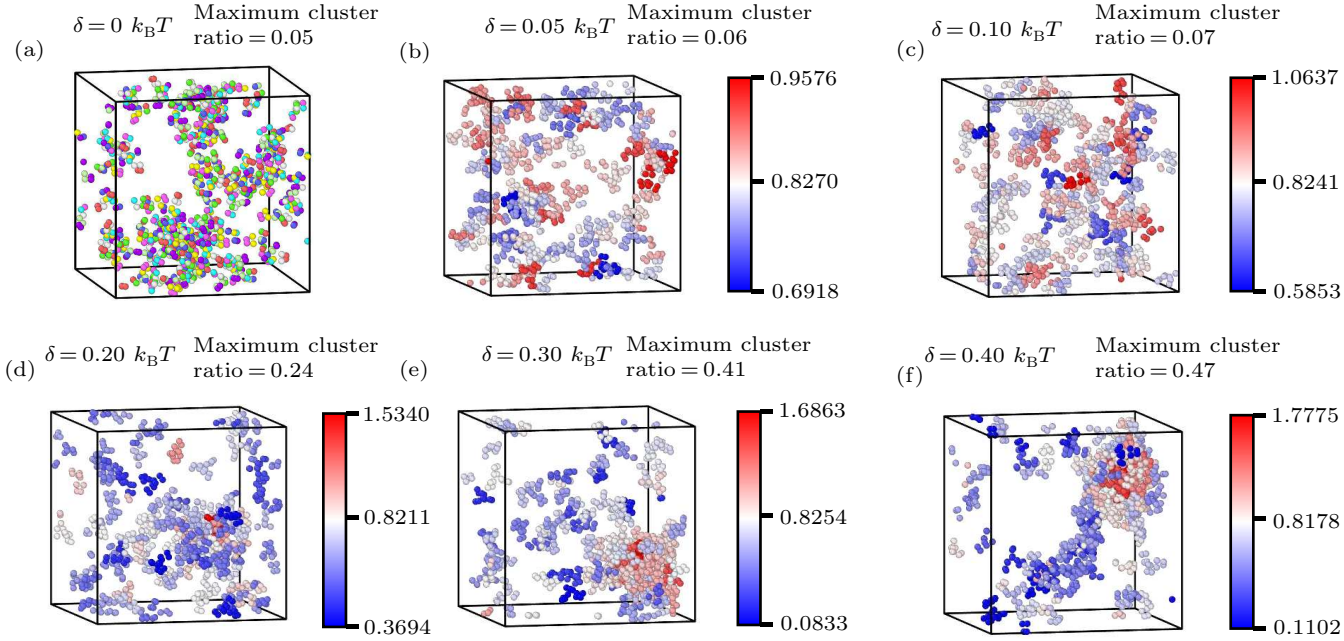


Fig. 9. The variation of the maximum cluster ratio and phase separation snapshots with the standard deviation at a temperature of $T = 255$ K. The intermolecular interaction strength in the IgG system has a mean value of 0.82 and standard deviations of (a) $0.00\ k_{\mathrm{B}}T$, (b) $0.05\ k_{\mathrm{B}}T$, (c) $0.10\ k_{\mathrm{B}}T$, (d) $0.20\ k_{\mathrm{B}}T$, (e) $0.30\ k_{\mathrm{B}}T$, and (f) $0.40\ k_{\mathrm{B}}T$. The color scale range varies from blue (weak interactions) to red (strong interactions). Clusters are defined using a distance-based criterion: two IgG molecules are considered part of the same cluster if any pair of interacting beads between them are within a cutoff distance of $2^{1/6}\sigma_{\mathrm{IgG}}$. The maximum cluster ratio is defined as the proportion of IgG molecules belonging to the largest cluster.

Local regions exhibit stronger interactions (red), suggesting that moderate energy dispersity has minimal impact on system stability. As the standard deviation further increases to 0.20 k_BT, 0.30 k_BT, and 0.40 k_BT, the ratio of the maximum cluster decreases to 0.72, 0.68, and 0.67, respectively. At this point, the energy map indicates that the regions of strong interaction (red areas) become more localized, while their overall distribution becomes more dispersed, leading to the formation of multiple smaller clusters.

The behavior of the IgG system at temperature $T =$ 255 K is illustrated in Fig. 9. When the standard deviation is 0.00 k_BT, the IgG system remains in a dispersed state, with the maximum cluster ratio as low as 0.05. As the standard deviation increases to 0.05 k_BT and 0.10 k_BT, the maximum cluster ratio slightly increases, and the system aggregates into multiple small clusters centered around regions of strong interactions (red). At a standard deviation of 0.20 k_BT, the IgG system forms a compact, large-cluster structure, with the maximum cluster ratio rising to 0.24. As the standard deviation continues to increase, the maximum cluster ratio significantly grows, ultimately reaching 0.47 when the standard deviation is 0.40 k_BT. This phenomenon indicates that the increase in standard deviation with gradual temperature rise facilitates phase separation in the system.

A detailed analysis of the effect of standard deviation variations on the maximum cluster ratio and the second-largest cluster ratio at different temperatures is provided in Fig. 10. At temperatures $T = 210$ K, molecular thermal motion is relatively weak, and the maximum cluster ratio remains stable, while the second-largest cluster ratio stays low. This suggests that under relatively low-temperature conditions, the majority of IgG molecules aggregate into a primary cluster, with others remaining widely dispersed, thereby limiting the formation of secondary clusters. In this context, smaller standard deviations favor the formation of maximum clusters (promoting phase separation). However, as the standard deviation of interaction strength increases, the complexity of IgG interactions increases, leading to a rapid decrease in the maximum cluster ratio. Under conditions where temperature exceeds 225 K, the maximum cluster ratio tends to increase as δ increases. This indicates that enhanced thermal motion at higher temperatures more effectively overcomes interaction barriers, facilitating the formation of larger clusters (i.e., higher standard deviations favor the formation of maximum clusters). The local aggregation effect thus becomes a dominant driving force for phase separation, increasing the likelihood of forming maximum clusters.

Overall, when the energy dispersity is large, IgG molecules with strong interactions remain stable despite temperature fluctuations. This stability contributes to a more consistent and robust cluster structure across the system. In more complex environments, such as real biological conditions where IgG interaction energies are more widely distributed, dispersity enhances the flexibility of molecular interactions, further promoting the formation of maximum clusters.

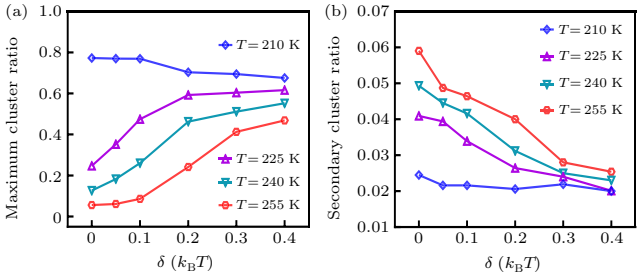


Fig. 10. The variations in (a) the maximum clusters ratio and (b) the second-largest cluster ratio with respect to standard deviation at different temperatures. The maximum cluster ratio is defined as the proportion of IgG molecules belonging to the largest cluster, and the secondary cluster ratio is defined as the proportion of IgG molecules in the second-largest cluster.

3.5. Effect of external polymer on IgG phase separation

In practical applications, IgG phase behavior is usually regulated by adding ions or polymer to IgG solutions.[71–73] Among these, polyethylene glycol (PEG) is mostly employed as a model system for studying excluded volume effects in protein phase separation research due to its distinctive non-adsorbing polymer characteristics.[74] To model such an exclusion mechanism, we implemented a purely repulsive Weeks–Chandler–Andersen (WCA) potential for the interaction between polymers and IgG. We systematically investigated the effects of varying concentrations of repulsive polymer on IgG phase separation. Figure 11(a) shows simulation snapshots of IgG phase separation ranging from 0 to 400 polymer molecules. As the number of polymer molecules increases, the extent of phase separation is enhanced, exhibiting a more distinct intermediate dense region at elevated polymer concentrations. Density distribution curves for polymer and IgG along the z-axis, obtained using the slab method, are shown in Figs. 11(b) and 11(c). The polymers exhibit higher densities at the sides and lower densities in the central region as their numbers increase. Upon adding polymer to IgG solutions, phase separation occurs immediately, and the IgG density in the intermediate region rises with polymer numbers. The coexistence densities of polymer and IgG under various conditions were calculated to construct the binary coexistence curve [Fig. 11(d)]. The effect of the polymer numbers on IgG phase separation is further demonstrated in Fig. 11(e), revealing that the dense-phase concentration of IgG increases with polymer numbers, indicating that polymer promotes IgG phase separation.[72]

Apart from PEG, other types of polymer (e.g., poly(L-lysine) (PLL))[75] are also used in experiments to regulate protein phase separation. These polymers may exert weak

attractive interactions with the IgG through various mechanisms. To further explore the impact of such attractive interactions between IgG and polymer on phase separation, we introduced Lennard–Jones (LJ) interactions (with interaction strength $\varepsilon = 0.1\ k_B T$) between the interaction sites of IgG (V_H, V_L, and C_{H3} regions) and the polymer. Under weak attractive conditions, we obtained binary phase separation snapshots and density distribution curves for polymer and IgG along the z-axis at different temperatures [Figs. 12(a)–12(c)]. The results demonstrated that low polymer numbers promoted IgG phase separation, consistent with findings observed with PEG. However, when the polymer numbers were increased further, the polymer significantly suppressed IgG phase separation, as evidenced by the marked decrease in dense-phase IgG concentration [Fig. 12(c)]. Using the slab method, we calculated the two-phase concentrations at various temperatures and fitted the coexistence curve, as shown in Fig. 12(d). The dual effect of polymer on IgG phase separation under weak attractive interactions is clearly illustrated in Fig. 12(e). This behavior is consistent with experimental studies indicating that additives interacting with the protein surface can reduce attractive protein-protein interactions, thereby diminishing the extent of protein phase separation.

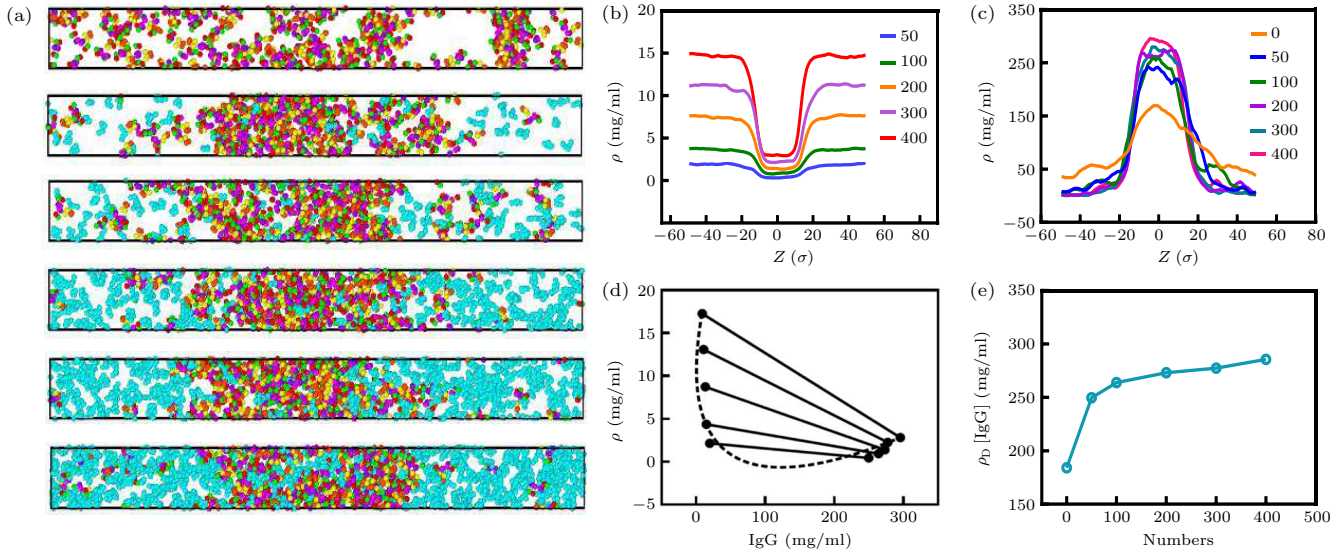


Fig. 11. The effect of different polymer numbers on the phase separation of IgG under conditions of purely excluded-volume interactions between IgG and polymer. (a) Phase separation snapshots of the IgG system at $T = 300$ K, with purely repulsive interactions between IgG and polymer, under polymer numbers of 0, 50, 100, 200, 300 and 400 molecules. Density distribution curves of (b) polymer and (c) IgG along the z-axis under different polymer numbers. (d) Coexistence curve of the IgG–polymer system. (e) The variation of IgG dense-phase density as a function of polymer numbers.

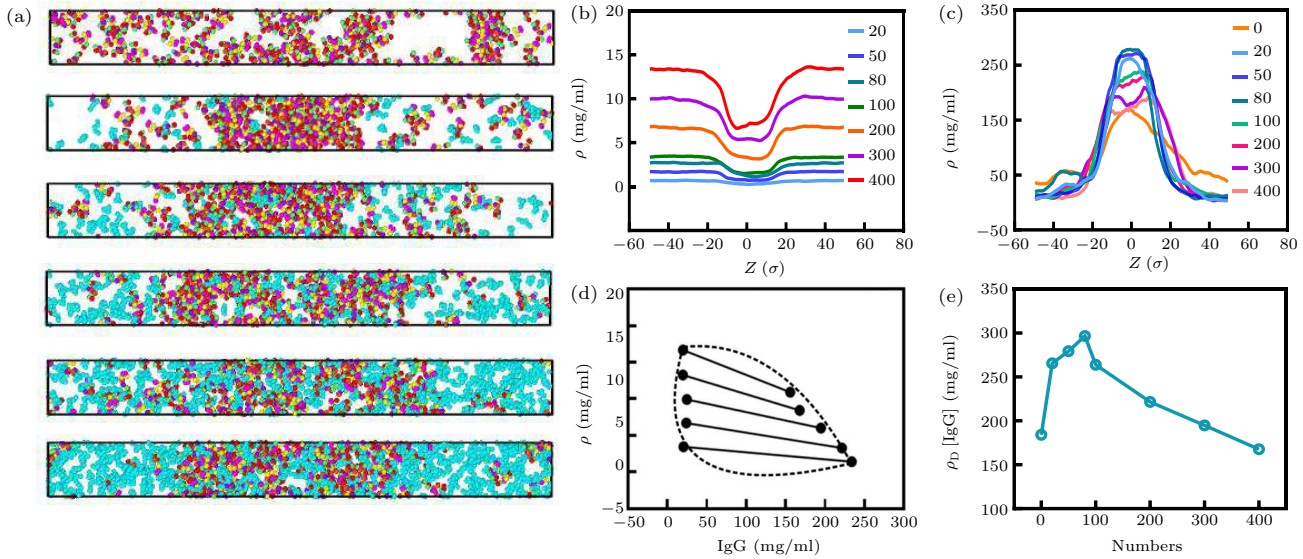


Fig. 12. The effect of different polymer numbers on the phase separation of IgG under conditions of weakly attractive interactions between IgG and polymer. (a) Phase separation snapshots of the IgG system at $T = 300$ K, with weakly attractive interactions between IgG and polymer, under polymer numbers of 0, 50, 100, 200, 300 and 400 molecules. Density distribution curves along the z-axis of (b) polymer and (c) IgG at different polymer numbers. (d) Coexistence curve of the IgG–polymer system. (e) The variation of IgG dense-phase density as a function of polymer numbers.

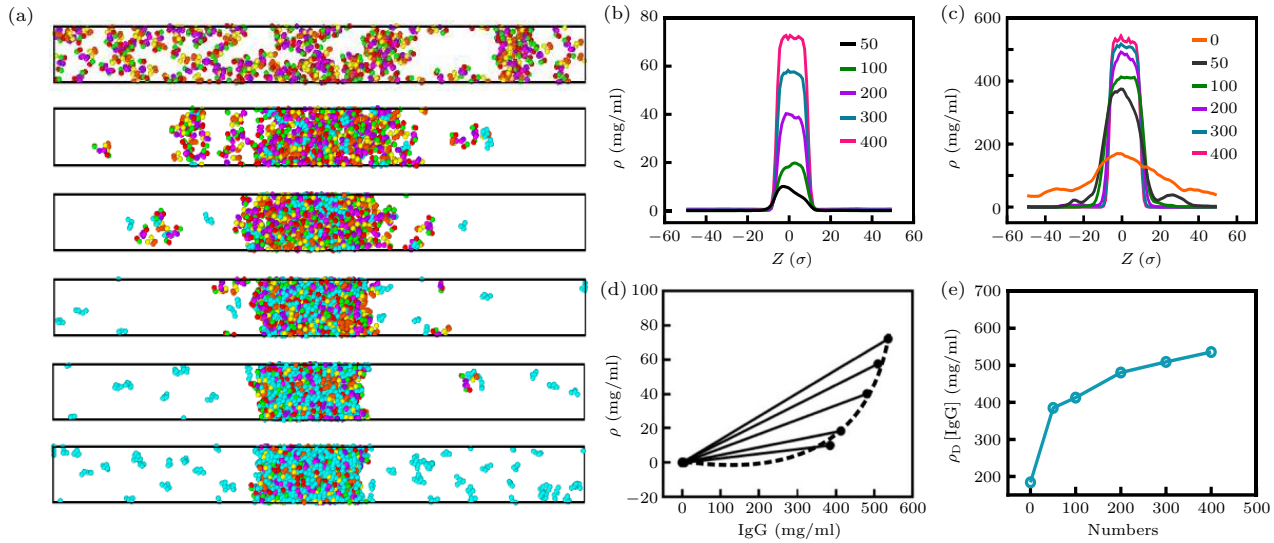


Fig. 13. The effect of different polymer numbers on the phase separation of IgG under conditions of strongly attractive interactions between IgG and polymer. (a) Phase separation snapshots of the IgG system at $T = 300$ K, with strongly attractive interactions between IgG and polymer, under polymer numbers of 0, 50, 100, 200, 300 and 400 molecules. Density distribution curves along the z-axis of (b) polymer and (c) IgG at different polymer numbers. (d) Coexistence curve of the IgG–polymer system. (e) The variation of IgG dense-phase density as a function of polymer numbers.

We further investigated the effect of strongly attractive polymers on IgG phase separation by increasing the interaction strength to 0.6 k_BT in the simulations. As shown in Fig. 13(a), under strongly attractive conditions, the IgG system transitions from a homogeneous state to a highly phase-separated state as the number of polymer molecules increases. Density distribution profiles of polymers and IgG along the z-axis obtained via the slab method [Figs. 13(b) and 13(c)] reveal that polymers are highly enriched within the dense IgG phase, and the volume fraction of the dense IgG phase exhibits an exponential increase with increasing polymer numbers, indicating that strong attractive interactions drive the formation of an intermolecular dynamic cross-linking network. Figure 13(d) shows that increasing polymer numbers significantly promote IgG aggregation and broaden the coexistence region. Figure 13(e) further quantifies the relationship between the density of the dense IgG phase and the number of polymer molecules, displaying a monotonically increasing trend, which confirms that adding strongly attractive polymer enhances IgG phase separation.

4. Conclusion

In summary, we utilized a partial-pair IgG coarse-grained molecular dynamics (CGMD) model to generate phase diagrams consistent with experimental data, and further provided valuable insights into the structural and material properties of IgG. A notable finding is the influence of dispersity in intermolecular interaction strengths on phase separation stability. We showed that higher standard deviations in interaction strengths lead to more stable phase-separated states, particularly under varying temperatures, underscoring the significance of diverse amino acid sequences in IgG's variable domains. We also explored the effects of external polymer. Our results indicated that increased polymer numbers promote phase separation through repulsive interactions. Additionally, we identified a dual regulatory effect with weakly attractive polymers (low concentrations enhance phase separation, while high concentrations inhibit it) and a monotonic effect with strongly attractive polymers. Overall, our study enhances the understanding of IgG phase separation at the molecular level, which contributes to the fundamental knowledge of IgG's biophysical properties and informs the design of therapeutic antibody formulations and biopharmaceutical products. Future studies should aim to bridge molecular-scale simulations with mesoscopic theories that explicitly account for domain-specific interactions and conformational flexibility. The development of continuum models, such as Flory–Huggins or φ-4 theory, that incorporate anisotropic interaction tensors may help better unify molecular mechanisms with macroscopic phase diagrams.

Acknowledgment

Project supported by the National Natural Science Foundation of China (Grant Nos. 12222506, 12347102, and 12174184).

References

[1] Edelman G M 1973 *Science* **180** 830
[2] Rosenberg A S 2006 *AAPS J.* **8** 59
[3] Vidarsson G, Dekkers G and Rispens T 2014 *Front. Immunol.* **5** 520
[4] Hatch H W, Bergonzo C, Blanco M A, Yuan G, Grudinin S, Lund M, Curtis J E, Grishaev A V, Liu Y and Shen V K 2024 *J. Chem. Phys.* **161** 094113
[5] Dumetz A C, Chockla A M, Kaler E W and Lenhoff A M 2008 *Biophys. J.* **94** 570

[6] Mason B D, Zhang-Van Enk J, Zhang L, Remmele R L Jr and Zhang J 2010 *Biophys. J.* **99** 3792
[7] Yan Z S, Ma Y Q and Ding H M 2024 *J. Chem. Phys.* **160** 064907
[8] Ren C L, Shan Y, Zhang P, Ding H M and Ma Y Q 2022 *Sci. Adv.* **8** eabo7885
[9] Pantuso E, Mastropietro T F, Briuglia M L, Gerard C J J, Curcio E, Ter Horst J H, Nicoletta F P and Di Profio G 2020 *Sci. Rep.* **10** 8902
[10] Larson N R, Wei Y, Cruz T A, Esfandiary R, Kalonia C K, Forrest M L and Middaugh C R 2023 *J. Pharm. Sci.* **112** 680
[11] Likhtman A E 2005 *Macromolecules* **38** 6128
[12] Nikoubashman A and Howard M P 2017 *Macromolecules* **50** 8279
[13] Demeule B, Lawrence M J, Drake A F, Gurny R and Arvinte T 2007 *Biochim. Biophys. Acta* **1774** 146
[14] Dorsaz N, Thurston G M, Stradner A, Schurtenberger P and Foffi G 2011 *Soft Matter* **7** 1763
[15] Sibanda N, Shanmugam R K and Curtis R 2023 *Mol. Pharm.* **20** 2662
[16] Herling T W, Invernizzi G, Ausserwöger H, Bjelke J R, Egebjerg T, Lund S, Lorenzen N and Knowles T P J 2023 *Proc. Natl. Acad. Sci. USA* **120** e2306700120
[17] Ausserwöger H, Krainer G, Welsh T J, Thorsteinson N, De Csilléry E, Sneideris T, Schneider M M, Egebjerg T, Invernizzi G, Herling T W, Lorenzen N and Knowles T P J 2023 *Proc. Natl. Acad. Sci. USA* **120** e2210332120
[18] Chen S, Lau H, Brodsky Y, Kleemann G R and Latypov R F 2010 *Protein Sci.* **19** 1191
[19] Nishi H, Miyajima M, Nakagami H, Noda M, Uchiyama S and Fukui K 2010 *Pharm. Res.* **27** 1348
[20] Ahamed T, Esteban B N A, Ottens M, Van Dedem G W K, Van Der Wielen L A M, Bisschops M A T, Lee A, Pham C and Thömmes J 2007 *Biophys. J.* **93** 610
[21] Mason B D, Zhang L, Remmele R L Jr and Zhang J 2011 *J. Pharm. Sci.* **100** 4587
[22] Nishi H, Miyajima M, Wakiyama N, Kubota K, Hasegawa J, Uchiyama S and Fukui K 2011 *J. Biosci. Bioeng.* **112** 326
[23] Trilisky E, Gillespie R, Osslund T D and Vunnum S 2011 *Biotechnol. Prog.* **27** 1054
[24] Wang Y, Lomakin A, Latypov R F, Laubach J P, Hideshima T, Richardson P G, Munshi N C, Anderson K C and Benedek G B 2013 *J. Chem. Phys.* **139** 121904
[25] Zheng Y, Li Q, Freiberger M I, Song H, Hu G, Zhang M, Gu R and Li J 2024 *J. Chem. Inf. Model.* **64** 6768
[26] Janc T, Korb J P, Lukšič M, Vlachy V, Bryant R G, Mériguet G, Malikova N and Rollet A L 2021 *J. Phys. Chem. B* **125** 8673
[27] Rao V S, Srinivas K, Sujini G N and Kumar G N S 2014 *J. Proteomics* **2014** 147648
[28] Jones S and Thornton J M 1996 *Proc. Natl. Acad. Sci. USA* **93** 13
[29] Nooren I M A and Thornton J M 2003 *Embo J.* **22** 3486
[30] Thompson R W Jr, Latypov R F, Wang Y, Lomakin A, Meyer J A, Vunnum S and Benedek G B 2016 *J. Chem. Phys.* **145** 185101
[31] Zhang F, Skoda M W A, Jacobs R M J, Martin R A, Martin C M and Schreiber F 2007 *J. Phys. Chem. B* **111** 251
[32] Antosiewicz J, Mccammon J A and Gilson M K 1994 *J. Mol. Biol.* **238** 415
[33] Voth G A 2017 *Acc. Chem. Res.* **50** 594
[34] Heyman B 2003 *Immunol. Lett.* **88** 157
[35] Brandt J P, Patapoff T W and Aragon S R 2010 *Biophys. J.* **99** 905
[36] Chaudhri A, Zarraga I E, Kamerzell T J, Brandt J P, Patapoff T W, Shire S J and Voth G A 2012 *J. Phys. Chem. B* **116** 8045
[37] Davies D R and Cohen G H 1996 *Proc. Natl. Acad. Sci. USA* **93** 7
[38] Wilson I A and Stanfield R L 1994 *Curr. Opin. Struct. Biol.* **4** 857
[39] Abhinandan K R and Martin A C R 2008 *Mol. Immunol.* **45** 3832
[40] Chothia C, Lesk A M, Tramontano A, Levitt M, Smith-Gill S J, Air G, Sheriff S, Padlan E A, Davies D, Tulip W R, Colman P M, Spinelli S, Alzari P M and Poljak R J 1989 *Nature* **342** 877
[41] Sivasubramanian A, Sircar A, Chaudhury S and Gray J J 2009 *Proteins* **74** 497
[42] Oganesyan V, Damschroder M M, Leach W, Wu H and Dallácqua W F 2008 *Mol. Immunol.* **45** 1872
[43] Oganesyan V, Damschroder M M, Woods R M, Cook K E, Wu H and Dallácqua W F 2009 *Mol. Immunol.* **46** 1750
[44] Hirschmann F, Lopez H, Roosen-Runge F, Seydel T, Schreiber F and Oettel M 2018 *J. Chem. Phys.* **148** 084112
[45] Harris J M, Martin N E and Modi M 2001 *Clin. Pharmacokinet.* **40** 539
[46] Brzezinski M, Argudo P G, Scheidt T, Yu M, Lemke E A, Michels J J and Parekh S H 2023 *bioRxiv* 570970
[47] Chudoba R, Heyda J and Dzubiella J 2017 *J. Chem. Theory Comput.* **13** 6317
[48] Wang Y, Latypov R F, Lomakin A, Meyer J A, Kerwin B A, Vunnum S and Benedek G B 2014 *Mol. Pharm.* **11** 1391
[49] Fetahaj Z, Jaworek M W, Oliva R and Winter R 2022 *Chem. Eur. J.* **28** e202201658
[50] Cruz R D C, Martins R J, Cardoso M J E D M and Barcia O E 2009 *J. Solut. Chem.* **38** 957
[51] Silmore K S, Howard M P and Panagiotopoulos A Z 2017 *Mol. Phys.* **115** 320
[52] Dignon G L, Zheng W, Kim Y C, Best R B and Mittal J 2018 *PLoS Comput. Biol.* **14** e1005941
[53] Thompson A P, Aktulga H M, Berger R, Bolintineanu D S, Brown W M, Crozier P S, Veld P J, Kohlmeyer A, Moore S G, Nguyen T D, Shan R, Stevens M J, Tranchida J, Trott C and Plimpton S J 2022 *Comput. Phys. Commun.* **271** 108171
[54] Wang H, Kelley F M, Milovanovic D, Schuster B S and Shi Z 2021 *Biophys. Rep.* **1** 100011
[55] Alshareedah I, Thurston G M and Banerjee P R 2021 *Biophys. J.* **120** 1161
[56] Kirkwood J G and Buff F P 1949 *J. Chem. Phys.* **17** 338
[57] Lee H, De Vries A H, Marrink S J and Pastor R W 2009 *J. Phys. Chem. B* **113** 13186
[58] Humbert M T, Zhang Y and Maginn E J 2019 *J. Chem. Inf. Model.* **59** 1301
[59] Tejedor A R, Collepardo-Guevara R, Ramírez J and Espinosa J R 2023 *J. Phys. Chem. B* **127** 4441
[60] Ramírez J, Sukumaran S K, Vorselaars B and Likhtman A E 2010 *J. Chem. Phys.* **133** 154103
[61] Boudara V a H, Read D J and Ramírez J 2020 *J. Rheol.* **64** 709
[62] Sundaravadivelu Devarajan D, Wang J, Szała-Mendyk B, Rekhi S, Nikoubashman A, Kim Y C and Mittal J 2024 *Nat. Commun.* **15** 1912
[63] Kastelic M and Vlachy V 2018 *J. Phys. Chem. B* **122** 5400
[64] Sagawa T, Oda M, Morii H, Takizawa H, Kozono H and Azuma T 2005 *Mol. Immunol.* **42** 9
[65] Raut A S and Kalonia D S 2016 *Mol. Pharm.* **13** 774
[66] Sun G, Wang Y, Lomakin A, Benedek G B, Stanley H E, Xu L and Buldyrev S V 2016 *J. Chem. Phys.* **145** 194901
[67] Yang L, Biswas M E and Chen P 2003 *Biophys. J.* **84** 509
[68] Widom B 1965 *J. Chem. Phys.* **43** 3892
[69] Williamson A R 1976 *Annu. Rev. Biochem.* **45** 467
[70] Henderson R, Watts B E, Ergin H N, Anasti K, Parks R, Xia S M, Trama A, Liao H X, Saunders K O, Bonsignori M, Wiehe K, Haynes B F and Alam S M 2019 *Nat. Commun.* **10** 654
[71] Annunziata O, Asherie N, Lomakin A, Pande J, Ogun O and Benedek G B 2002 *Proc. Natl. Acad. Sci. USA* **99** 14165
[72] Wang Y and Annunziata O 2007 *J. Phys. Chem. B* **111** 1222
[73] Arakawa T and Timasheff S N 1985 *Biochemistry* **24** 6756
[74] Bhat R and Timasheff S N 1992 *Protein Sci.* **1** 1133
[75] Nobeyama T, Furuki T and Shiraki K 2023 *Langmuir* **39** 17043